Optical Fiber Technology 97 (2026) 104497

Contents lists available at ScienceDirect

Optical Fiber Technology

journal homepage: www.elsevier.com/locate/yofte

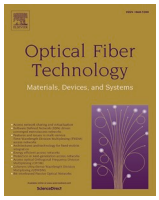

Regular Articles

Steady state radiation responses of graded-index germanosilicate multimode optical fibers

R. Pecorella [a,c,*], A. Morana [a], A. Boukenter [a], M. Cannas [c], Y. Ouerdane [a], S. Girard [a,b,*]

[a] Université Jean Monnet Saint-Etienne, CNRS, Institut d'Optique Graduate School, Laboratoire Hubert Curien UMR 5516, F-42023 Saint-Etienne, France
[b] Universitaire de France (IUF) Ministère de l'Enseignement Supérieur et de la Recherche, 1 rue Descartes 75005 Paris, France
[c] Dipartimento di Fisica e Chimica dell'Università degli Studi di Palermo I-90123 Palermo, Italy

ARTICLE INFO

Keywords:
RIA
Point defects
Optical fibers
Radiation-induced attenuation
Dose rate
Radiation effects

ABSTRACT

This study investigates the radiation response of commercially available germanosilicate graded-index multimode optical fibers (conforming to the OM1 through OM5 standards) at room temperature. The main objective is to monitor the radiation induced attenuation (RIA) and to identify the point defects at its origin, their generation and recombination mechanisms. The samples were irradiated under continuous X-ray exposure at two dose rates, 0.6 Gy/s and 6 Gy(SiO_2)/s, up to total ionization doses of 52 kGy and 109 kGy, respectively. The RIA kinetics at 850 nm, 1310 nm, and 1550 nm exhibited rapid initial growth followed by either a slower increase or a plateau, reflecting the interplay of defect generation, recombination, and conversion. OM2 through OM5 optical fibers showed a similar response with lower RIA compared to OM1 optical fiber, which justifies restricting the deeper analysis to OM1 and OM5 samples. Spectral decomposition of the RIA spectra shows that the dominant contributors are GeX and GeY at 850 nm; GeY and an unidentified band at 1310 nm; and Ge-STH together with the same unidentified band at 1550 nm. Moreover, GeX and GeY defects are the most dose rate sensitive defects, with their amplitudes nearly doubling at 6 Gy/s. The results obtained can be exploited to determine the potential of these Telecom-grade fibers for harsh environments with limited radiation constraints.

1. Introduction

Optical fiber (OF)-based technologies are increasingly being adopted across a wide range of application fields, owing to the numerous advantages they offer over conventional technologies. These include low intrusiveness due to their small size and weight, immunity to electromagnetic interference, high multiplexing capacity, and high bandwidth, among others. OFs are generally classified into two main categories: single-mode fibers (SMFs) and multimode fibers (MMFs). The former has a significantly smaller core diameter (typically around 9 μm) and supports the propagation of only the fundamental mode of light, provided the operating wavelength is above a certain cut-off. The latter features a larger core diameter (usually 50 or 62.5 μm), supports multiple light propagation modes, and, while generally MMF-based data links are more cost-effective than SMF-based ones, MMF offers lower bandwidth capacity. For this reason, in telecommunication applications, MMFs are typically used for short-haul links, enabling transmission distances of up to approximately 550 m at 10 Gbit/s. For longer distances, SMFs, primarily operating at 1310 nm or 1550 nm, are generally preferred [1]. The reduced bandwidth capacity of MMFs is primarily due to modal dispersion, which can be mitigated by employing graded-index (GI) rather than step-index (SI) multimode fibers. In GI fibers, a precisely engineered refractive index (RI) profile serves to equalize the group velocities of the guided modes, significantly reducing dispersion. To classify the capacity of GI-MMFs to support high data rates, five standards, OM1 through OM5, have been established [1,2,3]. OM1 fibers, with their 62.5 μm core diameter, represent the original multimode standard, supporting 10 Gbit/s Ethernet links up to approximately 33 m. The subsequent OM2 to OM5 fibers all share a 50 μm core but are distinguished by progressively lower intrinsic losses and higher bandwidth at the Telecom wavelengths. At 10 Gbit/s, OM2 supports data links up to ~ 82 m, OM3 up to ~ 300 m, and OM4 up to ~ 550 m. OM5 offers the same bandwidth and signal loss characteristics as OM4, while also enabling four-wavelengths multiplexing in the 850–940 nm window, boosting aggregate data capacity.

Some application areas, such as medicine, space, the nuclear industry, and high-energy physics [4,5,6,7], expose OFs to ionizing radiation, which, as widely documented in the literature, can lead to varying

* Corresponding authors.
E-mail addresses: roberto.pecorella@univ-st-etienne.fr (R. Pecorella), sylvain.girard@univ-st-etienne.fr (S. Girard).

https://doi.org/10.1016/j.yofte.2025.104497
Received 23 September 2025; Received in revised form 4 November 2025; Accepted 20 November 2025
Available online 3 December 2025

degrees of performance degradation depending on the radiation resistance of the fibers [8]. In this context, the primary macroscopic effect in silica-based OFs is radiation-induced attenuation (RIA). RIA manifests as excess transmitted signal loss due to the formation of radiation-induced point defects (color centers) inside the pure or doped silica core and cladding of the fibers [9,10]. These defects introduce energy levels within the silica bandgap, causing absorption of light at wavelengths to which the fibers would otherwise remain transparent [8].

In this study, we compare the radiation response of commercially available GI-MMFs, from OM1 to OM5, produced by the same manufacturer. These fibers are not radiation-hardened, and their RI profiles are primarily controlled by varying the germanium (Ge) dopant concentration in the core. In particular, Ge doping raises the core's refractive index above that of the pure-silica cladding, thereby satisfying the requirement for light guidance. Although phosphorus is sometimes used as a co-dopant in commercial optical fibers, to increase the refractive index and lower the melting temperature [11], it is not present in the fibers under test.

This investigation builds on a previous study conducted by our group on commercially available SMFs, which highlighted how the evolution of the fiber manufacturing techniques, pushed by the telecommunication market, could strongly affect the fiber radiation response [12]. In this case, our objective is to determine how irradiation dose rate influences the fibers' radiation response at room temperature (RT), specifically in terms of RIA, and to investigate how this effect manifests through the generation and evolution of the point defects responsible for the observed excess signal loss. As a result of the competition between the generation and recombination of point defects, the RIA is in fact sensitive to dose rate. At lower dose rates, thermally unstable defects have more time to recombine compared to higher dose rates. Consequently, for most types of optical fibers, RIA levels increase with dose rate at a given total ionizing dose (TID) [8,13,14,15].

With this goal in mind, we conducted online spectral RIA measurements in the visible (VIS) to infrared (IR) range, including telecommunication windows, under steady state X-rays at two distinct dose rates, up to the largest doses we could target with such optical fibers, around 100 kGy(SiO_2).

2. Materials and methods

2.1. Optical fibers under test

The samples studied in this work are GI-MM silica-based OFs with germanium-doped cores, conforming to the OM1 through OM5 standards. Table 1 reports their intrinsic attenuation at 850 nm and 1300 nm, two key telecommunication windows, along with their bandwidths and geometric dimensions, as provided by the manufacturer.

One of the main differences among these fibers lies in their refractive index profiles, as shown in Fig. 1. In particular, OM2 through OM5 exhibit nearly identical profiles, while OM1 stands out: all fibers except OM1 exhibit a refractive index dip located approximately 25 μm from the core center (radial distance 0 μm).

This feature is attributable to the presence of the co-dopant fluorine (F), as previously confirmed via energy-dispersive X-ray spectroscopy (EDX) measurements [16]. Fluorine co-doping is known to decrease the refractive index of silica. Interestingly, although OM1 and the other fibers differ in core size, the doped region extends to the same diameter, 62.5 μm, in all cases.

Table 1
Main characteristics of the optical fibers under test. Bandwidth values correspond to overfilled-launch bandwidth measured at 850 nm.

Sample	Fiber diameter (μm)	Core diameter (μm)	Attenuation @850 nm (dB/km)	Attenuation @1300 nm (dB/km)	Bandwidth (MHz•km) @850 nm
OM1	125	62.5	2.8	0.6	200
OM2	125	50	2.2	0.5	700
OM3	125	50	2.2	0.5	1500
OM4	125	50	2.2	0.5	3500
OM5	125	50	2.2	0.5	3500

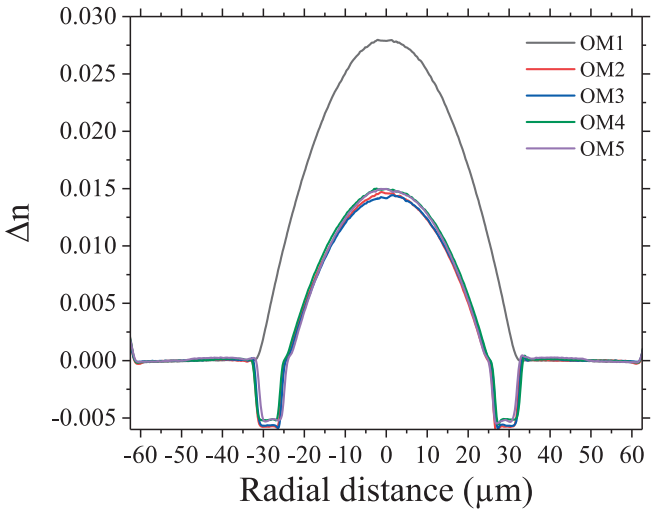

Fig. 1. Refractive index profiles of the fibers under test: OM1 (black), OM2 (red), OM3 (blue), OM4 (green), and OM5 (violet). The index modulation Δn is expressed relative to the RI of pure silica.

2.2. Irradiation characteristics

The fibers under test (FUT) have been irradiated, at room temperature, under X-rays at the IDFix facility, located at the Hubert Curien Laboratory in Saint-Étienne, France. The setup employs a 100 kV X-ray tube with a tungsten target, producing photons with a mean energy fluence of approximately 40 keV [17]. All the reported doses and dose rates refer to SiO_2. Irradiations were carried out at two dose rates, 0.6 Gy/s and 6 Gy/s, resulting in TIDs of 52 kGy and 109 kGy, respectively. In both cases, the dose homogeneity across the samples was verified using a calibrated ionization chamber and was found to be better than 6 %.

2.3. Experimental setup

To measure RIA in both visible and IR ranges during steady state X-ray irradiation and to continue monitoring the transmitted signal for two hours post-irradiation, the tested samples were arranged in monolayer coils to maximize the spatial homogeneity of the dose rate. For the irradiation runs at a dose rate of 0.6 Gy/s, each sample measured 40 m for IR and 5 m for VIS measurements; at 6 Gy/s, the lengths were 25 m for IR and 5 m for VIS. As shown in the schematic representation in Fig. 2, each sample was spliced to two radiation-resistant MM transport

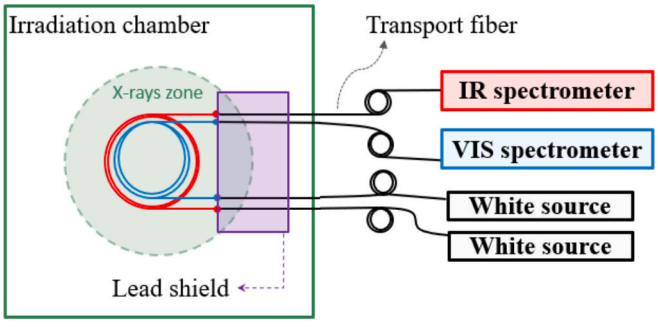

Fig. 2. Schematic representation of the experimental setup.

fibers shielded with lead. One of the transport fibers was connected to a light source, equipped with halogen-deuterium lamps, while the other one was connected to a spectrometer. Both the light source and spectrometers were from Ocean Optics: the QE65000 for the visible range (200–988 nm) and the NIRQuest for the infrared range (900–2137 nm).

3. Results

Fig. 3 reports the RIA kinetics at 850 nm (a,b), 1310 nm (c,d) and 1550 nm (e,f) as a function of dose (bottom x-axis) and time after the end of irradiation (top x-axis) for all the fibers. The data collected at the dose rate of 0.6 Gy/s are shown on the left, and those at 6 Gy/s on the right. It is evident that, at the lower dose rate, the radiation responses of the OM2 through OM5 fibers are very similar, with variations of less than 30 % at 850 nm, 7 % at 1310 nm, and 4 % at 1550 nm. Additionally, the RIA levels of OM1 are consistently higher, approximately twice those of the other fibers, throughout most of the irradiation period, across both dose rates and all wavelengths considered. During irradiation, at 1310 nm (Figs. 3c and d) and 1550 nm (Figs. 3e and f), the RIA increases rapidly during the initial few kilograys of accumulated dose, followed by a more gradual rise that continues until the end of the irradiation. At 850 nm, the RIA kinetics follow a distinct trend (Figs. 3a and b). At 0.6 Gy/s (Fig. 3a), after reaching around 5 kGy, the RIA remains nearly constant throughout the rest of the irradiation, a behavior typical of Ge-doped fibers [18]. The distinct radiation response is even more pronounced at the higher dose rate of 6 Gy/s (Fig. 3b), where the RIA, after initially increasing (up to ~6 kGy for OM1 and ~12 kGy for the others), subsequently decreases. These varying trends result from competing processes occurring during irradiation, such as the generation of radiation-induced defects (which increases RIA at wavelengths

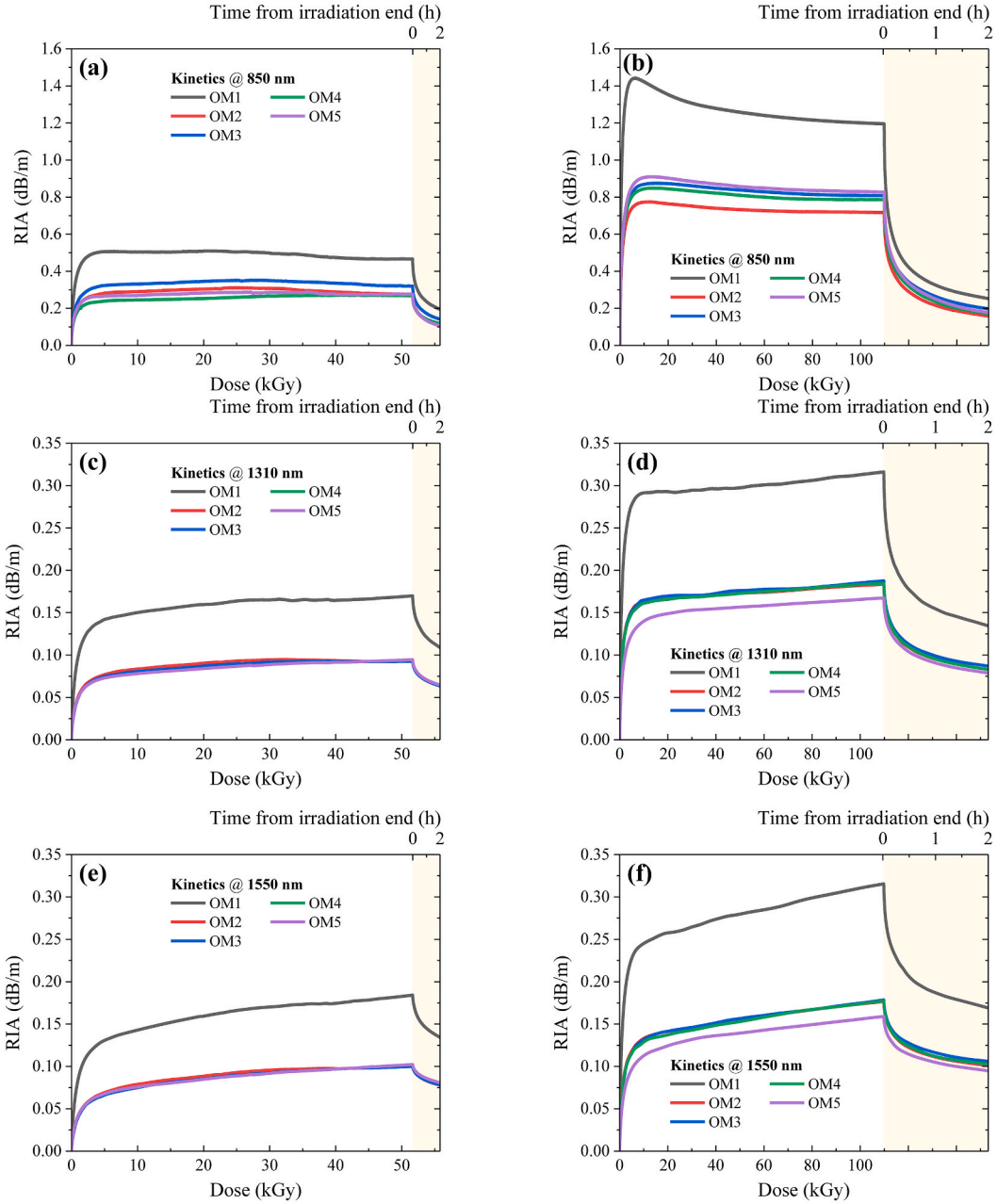

Fig. 3. RIA at 850 nm (a and b), at 1310 nm (c and d), at 1550 nm (e and f) as a function of dose (bottom x-axis) and time after the end of irradiation (top x-axis) for the fibers under test: OM1 (black), OM2 (red), OM3 (blue), OM4 (green), and OM5 (violet). The dose rate is 0.6 Gy/s for the graphs on the left and 6 Gy/s for those on the right. The faded yellow region indicates the two-hours recovery period following the end of each irradiation.

overlapping with their optical absorption (OA) bands), defect recombination (which reduces OA and then RIA at specific wavelengths), and defect conversions [8]. It is clear that, for both dose rates, the radiation responses of the OM2 through OM5 fibers are essentially the same. These fibers are less radiation sensitive than the OM1 fiber. This allows for a simplification of the data analysis, presented in the following section, by focusing on OM1 and a single representative fiber from the others, such as OM5, although the entire fiber set was tested. The kinetics shown in Figs. 3d and 3f reveal a difference of approximately 10 % between the curves of OM2–OM4 and OM5, although it is difficult to assess whether this difference is truly significant. In the two hours following the end of the irradiation runs (indicated by the yellow faded areas in Fig. 3), RIA levels drop with kinetics depending on fiber type, wavelength and dose rate. At 850 nm, the recovery percentage is similar for OM1 and the other fibers, averaging around 58 % at 0.6 Gy/s and 78 % at 6 Gy/s. Conversely, at 1310 nm and 1550 nm, OM1 exhibits greater recovery than the other fibers. At 0.6 Gy/s, OM1 recovers 36 % at 1310 nm and 27 % at 1550 nm, compared to 31 % and 22 % for the others. At 6 Gy/s, the recovery reaches 57 % and 46 % for OM1, while the other fibers recover 54 % and 42 %, respectively.

To investigate the evolution of RIA during irradiation at both dose rates, Fig. 4 (a-e) presents the RIA spectra (i.e., RIA as a function of wavelength) of all the fibers at three different dose levels (see Fig. 3 for reference): one during the initial phase of rapid RIA growth, one near the inflection point of the kinetics, and one at the end of the 0.6 Gy/s irradiation. Fig. 4f shows the kinetics at 0.6 Gy/s for OM1 and OM5 at the three wavelengths of interest, highlighting that OM1 consistently exhibits higher RIA levels than the other fibers (OM5 being representative) over the whole tested spectrum. Overall, the RIA curves obtained at 0.6 Gy/s lie below those at 6 Gy/s, suggesting that the dose rate influences the fibers' radiation response. Shortly after the start of irradiation (at 0.3 kGy), the RIA in the visible range is more than an order of magnitude

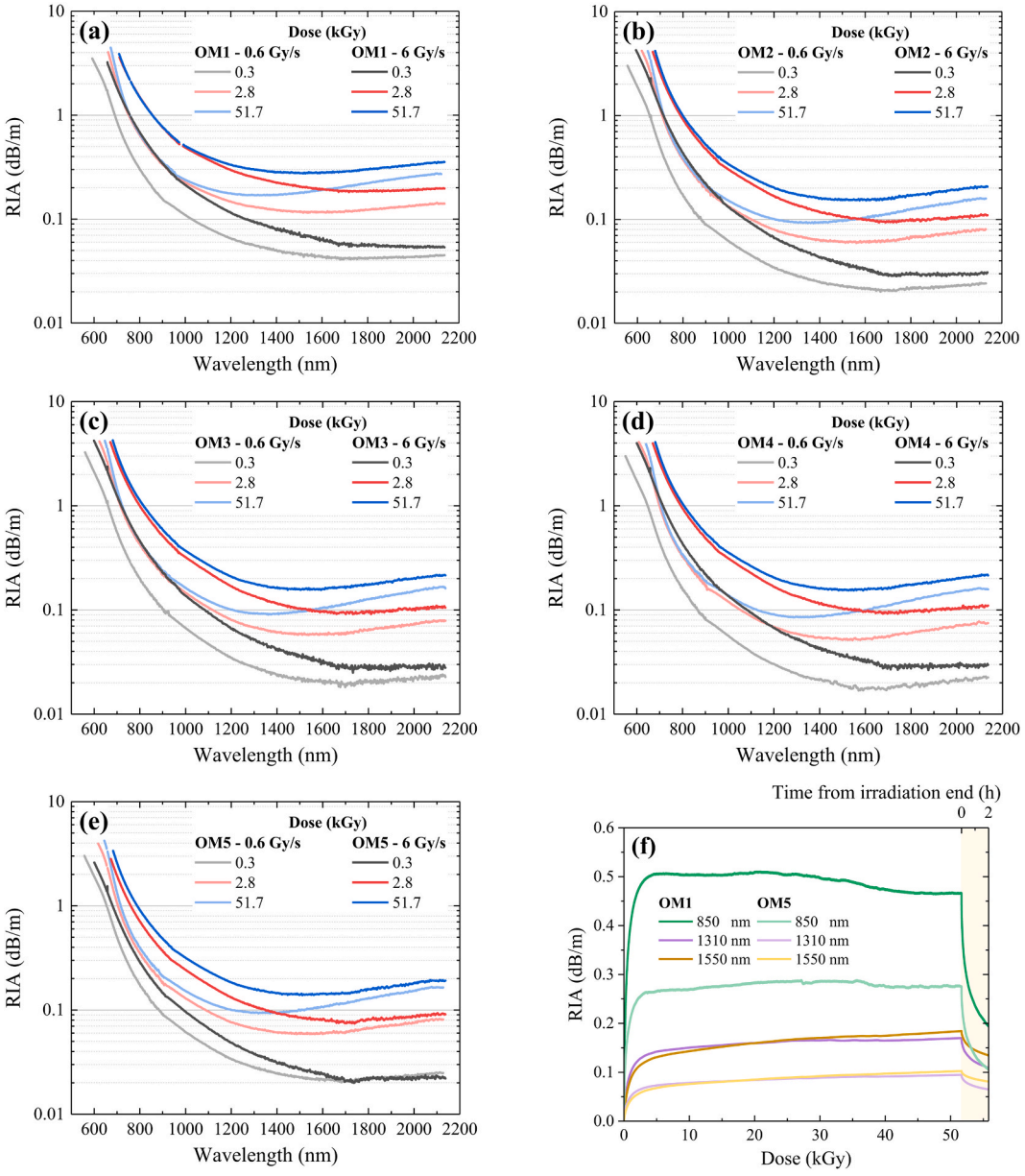

Fig. 4. RIA spectra measured for all the investigated samples at both dose rates, 0.6 Gy/s (light colors) and 6 Gy/s (medium colors), displayed on a semi-logarithmic scale at the TIDs of 0.3 kGy (gray), 2.8 kGy (red), and 51.7 kGy (blue). Panel (f) shows the RIA kinetics of OM1 (medium color) and OM5 (light color) as a function of dose (bottom x-axis) and time after the end of irradiation (top x-axis) at wavelengths of 850 nm (green), 1310 nm (magenta), and 1550 nm (yellow). The yellow region corresponds to the two-hours recovery period following the end of irradiation (corresponding to 51.7 kGy).

larger than in the infrared. In the case of 0.6 Gy/s, the RIA in the infrared reaches a minimum at around 1700 nm and then gradually increases beyond this wavelength, whereas at 6 Gy/s it remains nearly constant across the same spectral range. Already at this early stage of irradiation, the RIA of OM1 is higher than that of the other fibers over the entire investigated spectral window. As the dose continues to accumulate, at 2.8 kGy and 51.7 kGy, the RIA curves further increase, particularly at both ends of the spectral range. This suggests the possible dose-dependent growth of absorption bands related to radiation-induced defects, centered below 500 nm and above 2100 nm. The different radiation responses of these two groups of fibers might be explained by different causes. One hypothesis is that the higher Ge doping in OM1, compared to the other fibers, may lead to a greater number of radiation-induced defects, as higher Ge content can introduce additional structural disorder or stress in the silica matrix, potentially contributing to the formation of defect precursors. However, it has also been shown that increasing the Ge concentration does not always correlate with a higher population of Ge-related defects, as the actual defect density may saturate or even decrease with the increasing dose under certain conditions [19]. Another hypothesis, which does not exclude the first, is that the presence of fluorine in the core-cladding interface of the OM2-OM5 fibers may reduce the generation efficiency of Ge-related defects in those regions. Indeed, fluorine has been shown to lower the number of strained bonds in the glass matrix, acting as precursor sites for the generation of defects such as non-bridging oxygen hole centers (NBOHCs) [20].

4. Discussion

To identify the absorption bands underlying the RIA spectra reported in Fig. 4(a–e), we performed a spectral decomposition, using the minimal number of Gaussian components associated with radiation-induced point defects known in germanosilicate glasses, as documented in the literature [21]. Table 2 lists the peak energies and full widths at half maximum (FWHM) of the Gaussian bands used in the decomposition. Here, STH denotes self-trapped holes, and “Unknown OA” denotes an unassigned optical absorption band required by the fit to reproduce the RIA spectra of germanosilicate optical fibers. Although additional defects such as GeE’ and Ge(2) are certainly generated under irradiation, they do not contribute to the measured RIA, as their optical absorption bands peak at shorter wavelengths.

Fig. 5(a–c) shows the decomposition of the RIA spectra at the same three dose levels previously considered, using the OM1 fiber irradiated at 0.6 Gy/s as an example. The percentage residuals between the measured data and the fitted total curves are below 6 %. As the dose increases, the available spectral range narrows because the RIA in the visible region becomes so significant that the transmitted signal approaches the noise level. As a result, the amplitude of the absorption bands peaking in this region, namely Ge-NBOHC, GeX, Ge(1), becomes less reliable as the dose increases. We then applied the same spectral decomposition to the attenuation curve recorded two hours into the recovery phase, as shown in Fig. 5d, which also includes the RIA curve at the end of irradiation for comparison. This overlay reveals that, once irradiation stops, the GeY defect undergoes significant recovery. In particular, because its entire OA band lies within our measured wavelength range, comparing the fitted Gaussian amplitudes before and after recovery shows that its contribution to the attenuation decreases by approximately 40 % over two hours. Furthermore, the defects that predominantly affect the RIA at the three telecommunication wavelengths are: GeX and GeY at 850 nm, Unknown and GeY at 1310 nm, and Ge-STH and Unknown at 1550 nm.

Table 2
Parameters of the Gaussian absorption bands associated with the defects used for the spectral decomposition of the RIA, taken from [21].

Defect	Band peak (eV)	FWHM (eV)
Ge-STH	0.54	0.35
Unknown OA	0.88	0.33
GeY	1.38	0.71
Ge-NBOHC	1.95	0.17
GeX	2.6	0.97
Ge(1)	4.4	1.2

We applied the same analysis to the data acquired at the other dose rate for OM1 and OM5, as well as to data at additional dose levels, enabling us to trace the defect kinetics shown in Figs. 5e and 5f. The Ge (1) kinetics are omitted from these graphs because the peak of its absorption band lies well outside the data wavelength range. Ge-NBOHC is likewise excluded, as its absorption band falls outside the range at most dose levels, and its contribution is much weaker than that of the other defects, making it difficult to reliably estimate its OA amplitude. Overall, across both dose rates and all investigated dose levels, the amplitudes of the Gaussian components are consistently higher in OM1 than in OM5. This agrees with our previous work [16], which showed that OM4 (equivalent to OM5) is more radiation-resistant than OM1, based on a study of room temperature stable defects responsible for the permanent RIA measured long after γ-ray irradiation. Moreover, in Figs. 5e and 5f, the kinetics of each defect follow the same trend at both dose rates, remaining essentially parallel as the dose increases. In all cases, a rapid growth is observed during the accumulation of the first few kilograys; after this initial phase, some defects continue to grow slowly for the remainder of the irradiation, while others reach a plateau. In particular, the Ge-STH and the unidentified absorption band continue to increase, whereas GeX and GeY remain substantially constant after reaching a TID of ~3 kGy. These behaviors agree with the observations reported by Morana et al. [22] regarding the kinetics of Ge-STH, GeX, and GeY in Ge-doped optical fibers under X-rays. Interestingly, our results show that the RIA contributions from GeX and GeY centers are consistently higher in OM1 than in OM5, with amplitude ratios around 1.7. This trend contrasts with the behavior reported by Kashaykin et al. [23], where GeX concentration increases and GeY concentration decreases with higher content of GeO_2. The discrepancy might be related to the fluorine doping present in OM5, which may alter the formation or stability of these centers, as previously discussed.

Concerning the dose rate influence, all kinetics obtained at 6 Gy/s lie above those at 0.6 Gy/s, as already noted in the previous section when comparing the RIA curves. As reported in previous studies [24,25], this behavior is attributed to the fact that, for shorter irradiation times at higher dose rates (to reach the same total dose), radiation-induced defects have less time to recover during exposure via either thermal annealing or photobleaching processes, leading to higher RIA levels.

In our analysis, GeX and GeY appear to be the most dose rate sensitive defects: for OM1 fibers, their plateau-level responses at 6 Gy/s were, on average, 2.7 and 2 times the values observed at 0.6 Gy/s; for OM5, the corresponding factors were 2.5 and 1.95.

5. Conclusion

In this work, we investigated the radiation responses of commercially available Ge-doped GI-MMFs, (OM1-OM5 standards) under steady state X-rays at RT and at two dose rates: 0.6 Gy/s and 6 Gy/s, up to TIDs of 52 kGy and 109 kGy, respectively.

The RIA kinetics at 850 nm, 1310 nm, and 1550 nm, all exhibited rapid growth during the first few kilograys of accumulated dose, followed by either a slow RIA growth or a plateau. This behavior highlights the interplay of competing processes during irradiation, such as defect generation, recombination, and conversion. Nevertheless, for both dose rates, the radiation responses of OM2 through OM5 were essentially identical and consistently lower than that of OM1, in agreement with our previous work [15], which showed that OM4 (equivalent to OM5) is more radiation-resistant than OM1. Overall, to the lowest dose rate corresponds the lowest RIA, confirming that the dose rate affects the fibers’ radiation response, likely because, at higher dose rates, radiation-

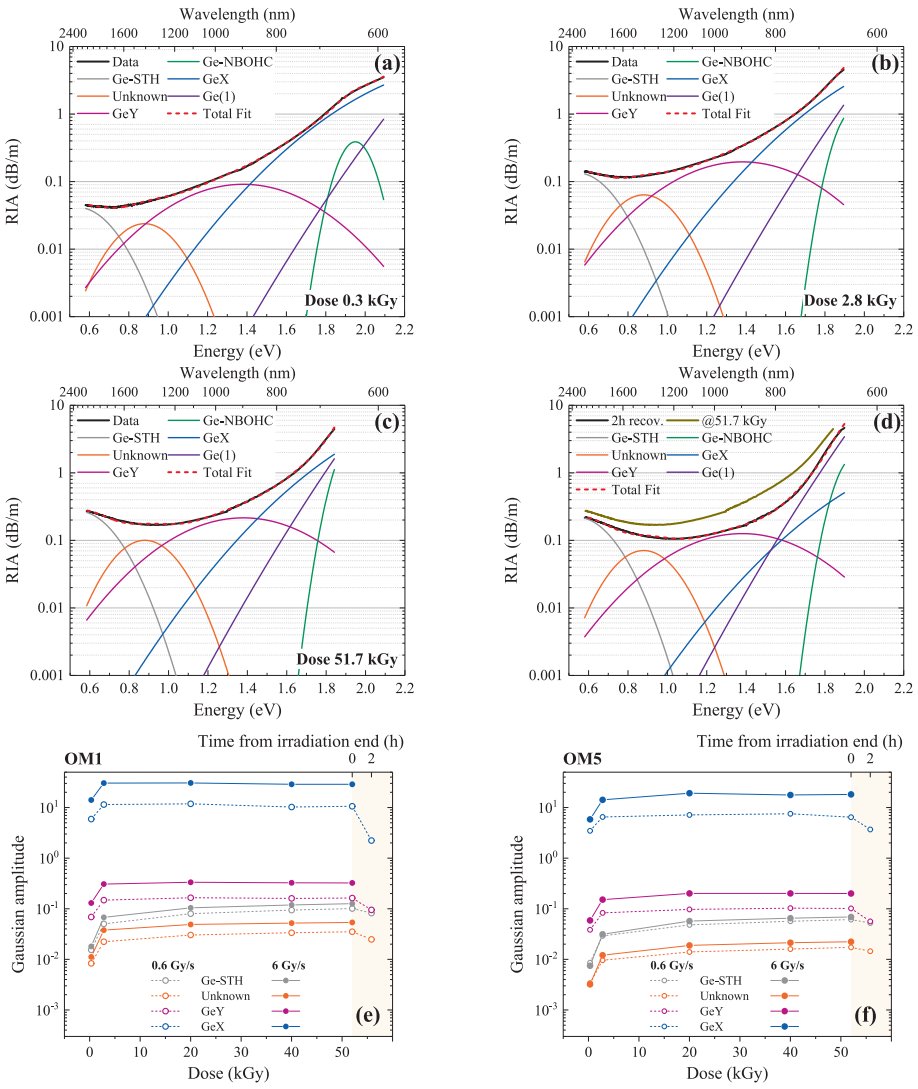

Fig. 5. (a–c) Spectral decomposition of the RIA spectra of OM1 irradiated at 0.6 Gy/s, at three dose levels: 0.3 kGy (a), 2.8 kGy (b), and 51.7 kGy (c), the latter corresponding to the end of irradiation. (d) Spectral decomposition of the attenuation curve recorded two hours after the end of irradiation. Spectra are plotted as a function of energy (bottom x-axis) and wavelength (top x-axis), using a semi-logarithmic scale. The measured spectra are shown in black, the total fit in dashed red, and the Gaussian components are: Ge-STH (gray), Unknown OA band (orange), GeY (magenta), Ge-NBOHC (green), GeX (blue), and Ge(1) (violet). (e,f) Amplitudes of the fitted Gaussian components as a function of dose (bottom x-axis), for OM1 and OM5, respectively, plotted on a semi-logarithmic scale. The yellow shaded region indicates the recovery period following the end of irradiation, with time shown on the top x-axis.

induced defects have less time to recover during exposure. By performing spectral decomposition of the RIA, we showed that the dominant contributors to the RIA at the three telecommunication wavelengths are: GeX and GeY at 850 nm, Unknown OA and GeY at 1310 nm, and Ge-STH and Unknown OA at 1550 nm.

The defect kinetics followed similar trends at both dose rates. In all cases, a rapid initial growth was observed within the first few kilograys, followed by either a slower increase or a plateau. In particular, Ge-STH and the unidentified absorption band continued to grow, while GeX and GeY stabilized after reaching a TID of approximately 3 kGy. Among the identified defects, GeX and GeY appeared to be the most dose rate sensitive, with their plateau amplitudes at 6 Gy/s nearly doubling those observed at 0.6 Gy/s. These behaviors are consistent with the trends reported in literature for Ge-doped fibers under X-rays. Furthermore, the consistently higher defect amplitudes observed in OM1 compared to OM2-OM5 may be related to their differing Ge and F doping levels, which can influence the density of defect precursors and the efficiency of defect formation.

These findings provide insight into the mechanisms driving RIA in Ge-doped GI-MMFs and highlight the importance of considering dose rate effects in radiation testing protocols.

CRediT authorship contribution statement

R. Pecorella: Writing – original draft, Investigation, Formal analysis, Data curation. **A. Morana:** Supervision. **A. Boukenter:** Supervision. **M. Cannas:** Supervision. **Y. Ouerdane:** Supervision. **S. Girard:** Writing – review & editing, Supervision, Project administration, Conceptualization.

Declaration of competing interest

The authors declare that they have no known competing financial interests or personal relationships that could have appeared to influence the work reported in this paper.

Data availability

Data will be made available on request.

References

[1] https://www.zion-communication.com/Differences-between-OS1-OS2-OM1-OM2-OM3-OM4-and-OM5-id3002360.html, Accessed on: November 18, 2024.
[2] ISO/IEC, 11801-1:2017, Nov. 2017.
[3] ANSI/TIA, 568.3-D, Oct. 2016.
[4] J. Blanc, et al., Characterization of radiation-resistant multimode optical fibers for large-scale procurement, IEEE Trans. Nucl. Sci. 68 (7) (2021) 1407–1413, https://doi.org/10.1109/TNS.2021.3074633.
[5] H. Henschel, et al., Effect of radiation on the bandwidth of graded index fibres, IEEE Trans. Nucl. Sci. 43 (3) (1996) 1018–1029, https://doi.org/10.1109/23.510750.
[6] E.A. Pospelova, et al., Radiation-resistant graded-index multimode optical fibers based on fluorosilicate glass, Tech. Phys. Lett. 49 (5) (2023) 39, https://doi.org/10.21883/TPL.2023.05.56025.19523.
[7] K. Sanada, T. Shamoto, K. Inada, Radiation resistance characteristics of graded-index fibers with a core of Ge-, F-doped or B and F-codoped SiO2 glass, J. Non Cryst. Solids 189 (3) (1995) 283–290, https://doi.org/10.1016/0022-3093(95)00233-2.
[8] S. Girard, et al., Overview of radiation effects on silica-based optical fibers and fiber sensors, IEEE Trans. Nucl. Sci. 72 (4) (2025) 982–1020, https://doi.org/10.1109/TNS.2024.3511455.
[9] S. Girard, et al., Radiation effects on silica-based optical fibers: recent advances and future challenges, IEEE Trans. Nucl. Sci. 60 (3) (2013) 2015–2036, https://doi.org/10.1109/TNS.2012.2235464.
[10] D.L. Griscom, A Minireview of the natures of radiation-induced point defects in pure and doped silica glasses and their visible/near-IR absorption bands, with emphasis on self-trapped holes and how they can be controlled, Phys. Res. Int. 2013 (1) (2013) 379041, https://doi.org/10.1155/2013/379041.
[11] G. Pacchioni, L. Skuja, D.L. Griscom (Eds.), Defects in SiO2 and related dielectrics: science and technology, Springer Netherlands, Dordrecht, 2000 doi: 10.1007/978-94-010-0944-7.
[12] A. Dufour, et al., Overview of the infrared radiation responses of telecom-grade single mode optical fibers, J. Lightwave Technol. 42 (14) (2024) 4987–4996, https://doi.org/10.1109/JLT.2024.3386025.
[13] A. Morana, et al., Temperature dependence of low-dose radiation-induced attenuation of germanium-doped optical fiber at infrared wavelengths, IEEE Trans. Nucl. Sci. 69 (3) (2022) 512–517, https://doi.org/10.1109/TNS.2021.3133421.
[14] F. Mady, M. Benabdesselam, J.-B. Duchez, Y. Mebrouk, S. Girard, Global view on dose rate effects in silica-based fibers and devices damaged by radiation-induced carrier trapping, IEEE Trans. Nucl. Sci. 60 (6) (2013) 4341–4348, https://doi.org/10.1109/TNS.2013.2282410.
[15] D.L. Griscom, M.E. Gingerich, E.J. Friebele, Radiation-induced defects in glasses: Origin of power-law dependence of concentration on dose, Phys. Rev. Lett. 71 (7) (1993) 1019–1022, https://doi.org/10.1103/PhysRevLett.71.1019.
[16] R. Pecorella, et al., Radiation effects on graded index germanosilicate multimode optical fibers, IEEE Trans. Nucl. Sci. (2025) 1, https://doi.org/10.1109/TNS.2025.3544020.
[17] A. Meyer, D. Lambert, A. Morana, P. Paillet, A. Boukenter, S. Girard, Simulation and optimization of optical fiber irradiation with X-rays at different energies, Radiation 3 (1) (2023) 58–74, https://doi.org/10.3390/radiation3010006.
[18] M. Van Uffelen, Modélisation de Systémes d'acquisition et de transmission à fibres optiques destinés à fonctionner en environnement nucléaire, Univ. Paris XI, Orsay, France, 2001. Ph.D. dissertation.
[19] I. Reghioua, et al., O2 loaded germanosilicate optical fibers: experimental in situ investigation and ab initio simulation study of GLPC evolution under irradiation, Appl. Sci. 12 (8) (2022), https://doi.org/10.3390/app12083916.
[20] L. Vaccaro, et al., Influence of fluorine on the fiber resistance studied through the nonbridging oxygen hole center related luminescence, J. Appl. Phys. 113 (19) (2013) 193107, https://doi.org/10.1063/1.4807163.
[21] S. Girard, et al., Overview of radiation induced point defects in silica-based optical fibers, Rev. Phys. 4 (2019) 100032, https://doi.org/10.1016/j.revip.2019.100032.
[22] A. Morana, M. Roche, E. Marin, A. Boukenter, Y. Ouerdane, S. Girard, Influence of hydrogen on the radiation-induced attenuation of ge-doped optical fibers, IEEE Trans. Nucl. Sci. 71 (4) (2024) 752–758, https://doi.org/10.1109/TNS.2024.3359859.
[23] P.F. Kashaykin, A.L. Tomashuk, V.F. Khopin, A.N. Guryanov, S.L. Semjonov, E. M. Dianov, New radiation colour centre in germanosilicate glass fibres, Quant. Electron. 48 (12) (2018) 1143–1146, https://doi.org/10.1070/QEL16850.
[24] A. Morana, et al., Extreme radiation sensitivity of ultra-low loss pure-silica-core optical fibers at low dose levels and infrared wavelengths, Sensors 20 (24) (2020) 7254, https://doi.org/10.3390/s20247254.
[25] S. Girard, et al., Recent advances in radiation-hardened fiber-based technologies for space applications, J. Opt. 20 (9) (2018) 093001, https://doi.org/10.1088/2040-8986/aad271.